Tie Line Framework to Optimize Non-Enveloped Virus Recovery in Aqueous Two-Phase Systems

Pratik U. Joshi[1], Dylan G. Turpeinen[1], Matthew Weiss[1], Glendy Escalante- Corbin[2], Michael Schroeder[1], Caryn L. Heldt[1*]
[1]Department of Chemical Engineering, Michigan Technological University
[2]Wayne County Community College District

[*]Corresponding Author: 1400 Townsend Dr., Houghton, MI 49931, USA
heldt@mtu.edu, phone 906-487-1134, fax 906-487-3213

Published as:
Joshi, P.U., Weiss, M., Corbin-Escalante, G., Schroeder, M.,and Heldt, C.L.[*]. (2019) Tie Line Framework to Optimize Non-Enveloped Virus Recovery in Aqueous Two-Phase Systems. Journal of Chromatography B. 1126-1127. 121744. doi: 10.1016/j.jchromb.2019.121744

Abstract

Viral particle purification is a challenge due to the complexity of the broth, the particle size, and the need to maintain virus activity. Aqueous two-phase systems (ATPSs) are a viable alternative for the currently used and expensive downstream processes. This work investigated the purification of two non-enveloped viruses, porcine parvovirus (PPV), and human rhinovirus (HRV) at various ATPS tie lines. A polyethylene glycol (PEG) 12kDa-citrate system at pH 7 was used to study the behavior of the partitioning on three different thermodynamic tie line lengths (TLLs). It was experimentally determined that increasing the TLL, and therefore increasing the hydrophobic and electrostatic driving forces within the ATPS, facilitated higher virus recoveries in the PEG-rich phase. A maximum of 79% recovery of infectious PPV was found at TLL 36 w/w% and TL ratio 0.1. Increased loading of PPV was studied to observe the change in the partitioning behavior and similar trends were observed for two different TLs. Most contaminants remained in the citrate-rich phase at all the chosen TLLs, demonstrating purification of the virus from protein contaminates. Moderate DNA removal was also measured. Net neutral charged HRV was studied to demonstrate the effects of driving forces on neutrally charged viruses. HRV recovery trends remained similar to PPV on each TLL studied, but the values were lower than PPV. Recovery of viral particles in the PEG-rich phase of the PEG-citrate system utilized the difference in the surface hydrophobicity between virus and proteins and showed a direct dependence on the surface charge of each studied virus. The preferential partitioning of the relatively hydrophobic viral particles in the PEG-rich phase supports the hypothesis that both hydrophobic and electrostatic forces govern the purification of viruses in ATPS.

Keywords: ATPS, virus purification, hydrophobicity, surface charge, salting-out

1. Introduction

The large number of new vaccines and gene therapy vectors coming to market has spurred growth in viral particle manufacturing. Vaccine manufacturing growth is also shifting to India and China [1], providing an opportunity to redesign currently approved processes for traditional vaccines. Since industries have yet to achieve a platform virus particle process, as has been achieved with antibody manufacturing [2], new unit operations need to be considered for viral products that can provide virus stability, high yields, and increased purity. The ultimate goals are to increase throughput, reduce production cost, and to shift towards continuous processing.

Two key attributes are hindering the manufacturing of viral particles, scale-up difficulties and low yield. In the laboratory, ultracentrifugation produces high purity and high concentration viral stocks [3, 4]. However, this extremely manual process is time consuming and expensive. In addition, co-precipitation has made sedimentation processes discouraging to be used for large-scale production of vaccines [5, 6].

The current race to develop a robust, easy to scale up, environmentally friendly and continuous process has led to tremendous research in various chromatography methods for viral particles. Commonly used chromatography modes for virus and viral vector processing include size exclusion [7-9], affinity [10, 11] and ion exchange [12, 13]. Although chromatography is a widely used method for purification of other biomolecules, low dynamic binding capacities of large biomolecules reduces the throughput and yield [14, 15]. The purification of rhinovirus using anion-exchange chromatography (AEX) found that only a fraction of viral particles bound to the column, leading to a high purity but low recovery process [16]. It was also observed that two peaks of virus eluted from the column, suggesting either different sites on the virus binding to the column or different sites on the column binding with different strength to the virus [16]. Issues of yield need to be addressed prior to large scale manufacturing of these viral particles.

A few studies have shown a continuous viral downstream process. Most commonly, a continuous simulated moving bed (SMB) configuration is used [17, 18]. Cell culture-derived influenza virus was purified with a three column SMB arrangement and a productivity of 3.8 times higher than batch mode was achieved [17]. However, the yield decreased from 80% in the batch mode to 70% in the SMB configuration and the purity decreased. A two column SMB chromatography system was used to purify adenovirus serotype 5 with size exclusion chromatography in a countercurrent configuration [18]. In this case, a higher yield was achieved in the SMB configuration (86%) as compared to batch mode (57%), with a 6-fold increase in the productivity. Although the integration of continuous chromatography is likely to reduce the overall cost and increase the productivity, the challenges pertaining to maintaining equipment robustness, sterility over long processing times, and real time process analytical technology (PAT) remain [19]. Due to these problems, the use of multiple columns still lack integration to the rest of the downstream processing units and is not currently used commercially [20].

Aqueous two-phase systems (ATPS) are potential candidates for virus purification to shorten the number of unit operations needed in the downstream processing train and provide simple integration into a continuous process. Unlike other purification methods, ATPS is robust, environmentally friendly, inexpensive, easy to scale up and can be operated as a continuous process with short processing times [21]. ATPS involves mixing two aqueous solutions which produce two phases when present above a critical concentration. Water is the major constituent (>70 w/w%) of each phase. Contrary to the high cost of chromatography resins and specialty membranes, the inexpensive raw materials used in ATPS, along with lower processing time and energy consumption, makes it a potential method to trim the cost of production for any biotherapuetic product [22]. A previous study of penicillin acylase purification compared ion exchange chromatography with ATPS, concluding that ATPS not only reduced the unit operation number from 7 to 4 but also lowered the gross production cost by 37%. The findings

were obtained considering 100 times re-use of the resin [23]. ATPS provides a good alternative for integrating clarification and purification for a more efficient downstream process.

Many types of ATPS have been developed to partition biomolecules. Examples include polymer/polymer [24], polymer/salt [25, 26], ionic liquid/salt [27, 28], and quaternary ammonium salt/salt [29] systems. The polymer/polymer system, typically polyethylene glycol (PEG) and dextran, is the classic ATPS. However, high viscosities, the expense of dextran, and the difficulty in polymer recycling led to the development of salt-containing systems. Polymer/salt systems have been extensively studied for protein purification [30-33]. But, there have been few studies on virus purification in ATPS. Some viruses and virus-like particles recovered by ATPS are shown in **Table 1**. Virus-like particles (VLPs) have been studied more often in ATPS to demonstrate a better downstream process for gene therapy vectors or subunit vaccines [25, 26, 34]. VLPs mimic the viral surface immunogenicity but are void of genomes [35]. Maintaining the infectivity of viruses is one of the major challenges in the downstream processes. This difference can be seen in the higher VLP recoveries as compared to the lower recoveries of infectious virus (**Table 1**).

ATPS have been run in continuous mode for the processing of protein products [39-41]. The relatively low viscosities and interfacial tension make the PEG-salt systems the preferred ATPS for scale up and continuous operation. Various methods to contact the two phases, such

Table 1. Overview of virus and virus-like particles in PEG/salt ATPS

Target Biomolecule	System	Recovery	Reference
Rotavirus-like particles	PEG 400/phosphate	90%	[26]
HIV-VLP	PEG 1500/sulfate	4.4*	[34]
Bacteriophage M13	PEG 400/ phosphate	83%	[36]
Bacteriophage T4	PEG 8000/phosphate	38%	[37]
Porcine parvovirus	PEG 12000/citrate	64%	[38]

*partition coefficient

as spray columns, perforated discs, pulsed cap columns, and conventional mixer-settlers have been suggested to perform continuous ATPS [39]. Mixer-settlers have successfully extracted monoclonal antibody (IgG1) [41] and an enzyme from spent yeast [40]. Some processing drawbacks such as flooding and backmixing have been identified [39]. But the problems are outweighed by the easy adaption of ATPS to continuous processes, as compared to chromatography. However, the complex partitioning mechanism of the biomolecules has averted the integration of ATPS at an industrial scale.

Numerous theories on the mechanism of partitioning of biomolecules in ATPS have been proposed. The two leading theories are that the partitioning is, 1) highly dependent on the excluded volume [30, 42-44], or 2) a combination of hydrophobic and electrostatic interactions [38, 45-47]. The excluded volume theory suggests that the random distribution of PEG molecules results in a geometrically saturated solution, excluding biomolecules from the polymer-rich phase due to a lack of space available for the biomolecule to occupy [48]. On the other hand, the hydrophobic and electrostatic interaction theory argues that the partitioning of the biomolecules is the combined effect of the salting-out from the salt-rich phase and a hydrophobic driving force pulling the biomolecule into the more hydrophobic PEG-rich phase [45]. Our data demonstrated that high MW PEG increased virus partitioning to the PEG-rich phase which supports the hydrophobic and electrostatic theory of partitioning [38].

The PEG and the salt composition and concentration control the hydrophobicity and electrostatics, respectively, in ATPS [49, 50]. High MW PEG stay more globular in solution than lower MW PEG, which are more linear in solution [49, 51]. Linear PEGs have more interaction with water and are better hydrated, whereas globular PEGs are less hydrated and therefore have more hydrophobic character. Unlike higher MW PEG, lower MW PEG have lower capabilities to provide multiple hydrophobic binding sites due to lower numbers of ethylene monomers [49]. For salts, the Hoffmeister series, which describes the hydration ability of

different ions, has been used to describe the effect of different salts in ATPS [38, 52]. A lower concentration of salt is required to form the two-phase region when multivalent salts are used as compared to monovalent salts [50], demonstrating the importance of ionic strength in the system. However, there are still many questions as to the driving forces within the ATPS that govern partitioning. Without a more systematic characterization of the two-phase region, ATPS will continue to have too many unknown variables that make it too risky to use in an FDA approved process.

This study aimed to determine the effect of PEG and salt concentration on virus recovery. The model non-enveloped viruses used for this study were porcine parvovirus (PPV), a single stranded DNA virus with a diameter of 18-26 nm [53], and human rhinovirus (HRV), a single stranded RNA virus with a diameter of ~30 nm [54]. Both virues have icosahedral symmetry. Previous work had established that the PEG 12kDa-citrate system could recover PPV in the PEG-rich phase [38]. This particular study focused on tie line characterization and its effect on PPV and HRV recovery to create a stronger theory on the mechanism of partitioning for viral particles in ATPS. Tie lines are thermodynamic equilibrium points that form in the two-phase region. Along a tie line, the system separates into phases that have the same concentration, but the volume ratio of the phases changes. This systematic evaluation of the two-phase ATPS space allowed us to understand the balance between the salting-out effect of the citrate-rich phase and the ability of the PEG-rich phase to pull the virus out of the interface and into the PEG-rich phase by hydrophobic interactions. It is difficult to recover biomolecules from the interface, so extracting as much virus into the PEG-rich phase was desired. There was a unique separation behavior observed at each tie line length (TLL). With a matrix containing TLL and tie line ratios, we were able to recover the majority of the infectious PPV in a PEG 12kDa-citrate system with high purity. By comparing the PPV recovery to the HRV recovery, we were able to add to the understanding of viral particle driving forces in ATPS.

2. Materials & Methods

2.1. Materials

Eagle's medium essential media (EMEM), sodium bicarbonate, phosphate buffered saline (PBS, pH 7.2), penicillin-streptomycin (10,0000 U/ml) and trypsin/EDTA for cell propagation were purchased from Life Technologies (Carlsbad, CA). Fetal bovine serum (FBS, Canada origin) was purchased from HyClone™ GE Healthcare (Pittsburg, PA). 3-(4,5-dimethyl-2-thiazolyl)-2,5-diphenyl-2H-tetrazolium bromide (MTT) was purchased from Alfa Aesar (Haverhill, MA) and sodium dodecyl sulfate (SDS) was purchased from VWR (Radnor, PA). Polyethylene glycol with an average molecular weight of 12000 (PEG 12kDa), trisodium citrate dihydrate (≥99%), anhydrous citric acid, and sodium phosphate dibasic heptahydrate (ACS reagent grade) were purchased from Sigma-Aldrich (St. Louis, MO). Sodium phosphate monobasic monohydrate (ACS reagent grade) was purchased from Fisher Scientific (Waltham, MA). All solutions were made with NANOpure water (Thermo Scientific, Waltham, MA) at a resistance of ≥18 MΩ and filtered with a 0.2 μm Nalgene (Thermo Scientific) bottle top filter prior to use.

2.2 Methods

2.2.1 Cell maintenance and virus titration

Porcine kidney cells (PK-13) and H1HeLa cells (HeLa), purchased from ATCC (CRL-6489™ and CRL-1958™ respectively), were grown in EMEM supplemented with 1% penicillin/streptomycin. In addition, the PK-13 cell media was supplemented with 10% FBS and the HeLa cell media was supplemented with 5% FBS. The cells were incubated at 37°C, 5% CO_2, and 100% humidity. PPV strain NADL-2 was a generous gift from Dr. Ruben Carbonell (North Carolina State University, Raleigh, NC), and was propagated in PK-13 cells, as described previously [55]. HRV-14 strain 1059 was purchased from ATCC (VR-284™) and propagated in HeLa cells. Briefly, HRV was infected at 0.001 MTT_{50}/cell after 24 hours of HeLa

incubation at 70-80% confluency. The infected HeLa cells were incubated at 35°C for HRV propagation. The cell lysis was collected 5 days post-infection.

The titer of PPV and HRV were found by the colorimetric MTT cell viability assay [56]. Briefly, 96-well plates were seeded with PK-13 or HeLa cells at a seeding density of $8x10^4$ cells/well. The cells were infected 24 hours post-incubation with PPV or HRV and serially diluted at a 1:5 ratio across the plate. PPV infected PK-13 cells were incubated at 37°C and HRV infected HeLa cells were incubated at 35°C. After six days, an MTT salt solution was added to each well and both cell lines were incubated at 37°C. This was followed by addition of an acidic SDS solubilization solution. The absorbance was recorded with a Synergy Mx microplate reader (BioTek, Winoski, VT) after 4-12 hours. The 50% infectious dose value of PPV and HRV was determined and reported in the units of MTT_{50}/ml [55].

2.2.2 Construction of binodal curves and tie lines

The binodal curve was generated using the turbidity method with appropriate stock PEG and citrate concentrations, as described earlier [38]. Briefly, systems were formed at high concentrations and diluted with water till the turbid systems turned clear.

The tie lines were determined by conductivity measurements of the citrate-rich (bottom) phase using a VWR® sympHony™ conductivity meter (Radnor, PA), [50] and intrapolating the citrate compositions from a standard curve. The endpoints of the tie lines were determined by calculating the remaining amount of citrate in the PEG-rich (top) phase by completing a mass balance of the system. The tie lines were characterized by their tie line length (TLL), calculated as [57],

$$TLL = \sqrt{\Delta x_{PEG}^2 + \Delta x_{salt}^2} \quad (1)$$

where Δx_{PEG} is the concentration difference of PEG in the top phase and bottom phase and

$\Delta x_{citrate}$ is the concentration difference of citrate in the top phase and bottom phase. Tie line ratios were calculated as

$$TL\ ratio = \frac{length\ (\overline{TS})}{length(\overline{SB})} \quad (2)$$

where *S* is the system composition point, *T* is the top node, and *B* is the bottom node (see **Figure 1**). The volume ratios were calculated as

$$VR = \frac{(Volume)_{top\ phase}}{(Volume)_{bottom\ phase}} \quad (3)$$

After determining the tie lines, TLL 15, 25, 36 w/w% were chosen for the study of virus partitioning. ATPSs were made with stock solutions of 30 w/w% citrate and solutions ranging from 33-45 w/w% of PEG. Appropriate amounts of stock solutions, water and 0.1g of crude PPV were added to a microcentrifuge tube to complete a 1g system. All systems were mixed with a vortex mixer and the phase separation was carried out in an ST16R Centrifuge (Thermo Scientific, Pittsburg, PA) at ~12,300 x*g* at 21°C for 5 min. The recovery of PPV was calculated as

$$\%\ Recovery = \frac{V_{P/C} * T_{P/C}}{V_i * T_i} * 100 \quad (4)$$

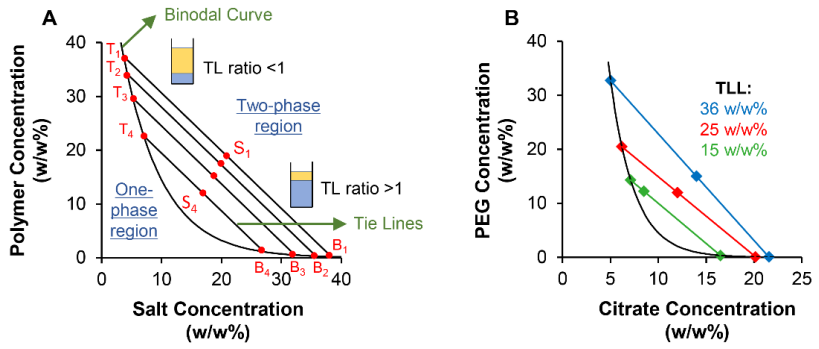

Figure 1. Binodal curve and tie lines. (A) Schematic illustration of ATPS showing binodal curve separating one-phase region from the two-phase region and set of systems characterized by tie lines and TL ratios. (B) Experimentally determined binodal curve and tie lines for PEG 12kDa-citrate ATPS at pH 7.

where *V* is the volume of the PEG-rich phase (*P*), the citrate-rich phase (*C*) or the initial stock (*i*) and *T* is the titer of one phase expressed as $\log_{10}$ MTT_{50}/ml [38]. The partitioning coefficient was calculated as

$$K = \frac{V_P * T_P}{V_C * T_C} \quad (5)$$

2.2.3 Physical Properties of Systems

The refractive index of the extracted PEG-rich phases was measured with a Digital Brix/RI-Chek refractometer (Reichert Technologies, Depew, NY), with an accuracy of ±0.0002. Densities of the PEG-rich and citrate-rich phases were measured by weighing 1 ml of the phase using a calibrated pipette on a Mettler-Toledo analytical balance (Columbus, OH), with a readability up to 0.1 mg.

2.2.4 SDS-PAGE

The partitioning of the contaminant proteins in the crude lysate was measured using sodium dodecyl sulfate-polyacrylamide gel electrophoresis (SDS-PAGE) with a 4-12% Bis-Tris NuPage gel and NuPage MOPS running buffer (Life Technologies, Carlsbad, CA). Benchmark™ protein ladder with a molecular weight range of 10-220 kDa (Life Technologies) was used as the marker. Samples were reduced using β-mercaptoethanol (Sigma-Aldrich, St. Louis, MO) at 7% concentration, and heated to 70°C for 10 min prior to loading onto the gel. The SDS-PAGE was run for 55 min at a constant 200 V. The gel was loaded at a constant volume so that concentrations of contaminating proteins could be compared. The gel was stained with the SilverXpress™ staining kit (Life Technologies, Carlsbad, CA).

2.2.5 DNA quantification

DNA content in the PEG-rich phase and citrate-rich phase was measured using the Quant-iT™ PicoGreen® dsDNA kit (ThermoFisher Scientific, Waltham, MA). The PEG-rich

phase and citrate-rich phase were diluted in water to have a final concentration of PEG and citrate as ≤1 w/w%. The host cell DNA in the crude lysate, PEG-rich and citrate-rich phase was measured, as per manufacturer's instruction. The fluorescent activities (excitation: 480 nm and emission: 520 nm) of the samples were measured using a Synergy™ Mx microplate reader. DNA recovery was calculated similar to virus recovery as:

$$\%\, DNA\ recovery = \frac{DNA\ concentration_{P/C} * V_{P/C} * DF}{DNA\ concentration_i * V_i * DF} * 100 \quad (6)$$

Where *V* denotes volume of the PEG-rich phase (*P*), citrate-rich phase (*C*) or initial stock (*i*) and *DF* denotes the respective dilution factor.

2.2.6 Dynamic Light Scattering (DLS)

Virus aggregates at varying concentrations of citrate were measured by DLS with a Malvern Zetasizer Nano ZS (Westborough, MA). First, virus was dialyzed in Biotech cellulose ester 1000 kDa dialysis tubing (Rancho Dominguez, CA) at 4°C for two days with two buffer exchanges of 20 mM phosphate buffer at pH 7.0 (PB). Then, the dialyzed virus was further purified in an Econo-Pac 10DG desalting column (Hercules, CA). The fraction containing the highest titer was used to mix with sodium citrate solution at pH 7 to give different final concentrations of citrate or added to the citrate-rich phase after ATPS separation. The hydrodynamic diameter was measured and the aggregate ratio (*AR*) was calculated as:

$$AR = \frac{D_{H,18-26nm}}{D_{H,>100nm}} \quad (7)$$

where $D_{H,20nm}$ is the maximum intensity of the peak at 18-26 nm (the virus intensity) and $D_{H,>100nm}$ is the maximum intensity of the aggregate peak, which was >100 nm and became larger as the concentration of citrate increased.

3. Results

Table 2. A brief description and comparison of the model viruses (PPV and HRV)

Model Virus	Genome	Family	Related Virus	Isoelectric Point	Size (nm)	References
Porcine Parvovirus (PPV)	ssDNA	parvoviridae	B19, AAV	5.0	18-26	[60, 63]
Human Rhinovirus (HRV)	(+)ssRNA	picornaviridae	FMDV, Polio, Hep A	6.9	~30	[64-66]

B19: B19 parvovirus; AAV: adeno associated virus; FMDV: foot & mouth disease virus; Polio: poliovirus; Hep A: hepatitis A virus

3.1. Model virus

Porcine parvovirus (PPV) and human rhinovirus (HRV) were chosen as the model non-enveloped viruses to study the partitioning in ATPS and key properties are shown in **Table 2**. PPV is a ssDNA virus that is approximately 18-26 nm in diameter [53]. PPV is a pathogenic agent that causes reproductive failure in swine populations [58, 59], and is a model for the human B19 parvovirus. The capsid of PPV is composed of three proteins, VP1, VP2, and VP3. VP2 is the major constituent (~80%) of the capsid [60]. Recently, a comparative study using computational and experimental methods showed that PPV [61] and a closely related murine parvovirus, MVM [62], are more hydrophobic than a panel of proteins. This significant difference in the surface hydrophobicity of PPV and contaminant proteins is an ideal driving force to develop new purification methods for viral particles.

HRV is a ssRNA virus that is ~30nm in diameter, composed of VP1, VP2, VP3, and VP4 capsid proteins [64, 66]. VP1, VP2, and VP3 are surface exposed antigenic proteins, whereas VP4 is present in the inside of the capsid and assists in anchoring the RNA inside the capsid [64]. HRV is one of the agents causing common cold and exacerbations of asthma in humans, with three main species, namely A, B, and C, and more than 100 serotypes identified [67-71]. Despite extensive research, there is no effective antiviral drug treatment for HRV infections [72]. This virus was used to show the effect of surface hydrophobicity at net neutral surface charge on virus partitioning in ATPS.

3.2. Binodal curves & tie lines

The ATPS binodal phase diagram separates the homogeneous region from the two-phase region, as shown in **Figure 1A**. Tie lines were generated to study systems containing the same concentrations of each component in the PEG-rich and citrate-rich phases. Tie lines are thermodynamic equilibrium states in the two-phase region, representing a unique value of Gibb's free energy [57, 73]. An increase in the TLL (**Eq. 1**) increases the Gibb's free energy, which correlates to the thermodyanmic driving force [73] and results in higher PEG and salt concentrations in each phase. Additionally, an increase in TLL also provides elevated hydrophobic interaction from the PEG-rich phase and effective salting-out of proteins from the salt-rich phase [74]. Increasing the TLL is hypothesized to provide a larger hydrophobic driving force for the partitioning of PPV and HRV into the PEG-rich phase.

Each system composition is represented by a tie line (TL) ratio (**Eq. 2**). The TL ratio is the ratio of a length of the segment from the system point to the top node divided by the length of the segment from the system point to the bottom node of that tie line [57]. The phase volumes change as the TL ratio changes, as shown in **Figure 1A**.

Earlier studies have shown that a PEG 12kDa-citrate system was able to separate and recover 64% of infectious PPV [38]. This is a higher MW of PEG than typically studied in PEG-salt ATPS. Although higher MW causes an increase in viscosity and interfacial tension [75, 76], it also elevates the hydrophobic driving force in the PEG-rich phase, which increased the virus recovery [38]. Hence, it was decided to study the PPV purification at varying tie lines in the PEG 12kDa-citrate system to better understand the effect of PEG and citrate concentration on virus recovery.

Several groups have generated binodal curves for polymer/salt systems [38, 77-80]. The phase diagram was experimentally determined for the PEG 12kDa-citrate system and can be seen in **Figure 1B**. Refractive index and density were also used to confirm the tie lines (see

Table 3. Comparison of TL ratio (Eq. 2) and volume ratio (Eq. 3)

System Composition		TLL (w/w%)	TL ratio	Volume ratio
PEG Conc. (w/w%)	Citrate Conc. (w/w%)			
30.0	6.4		0.1	7.7
15.0	14.0	36	1.2	0.9
10.0	16.5		2.3	0.4
18.5	7.5		0.1	3.7
10.3	13.2	25	1.0	0.5
6.2	16.0		2.3	0.3
13.7	7.5		0.1	0.8
7.4	11.8	15	1.0	0.4
4.6	13.6		2.3	0.3

Table S1 and **S2**). The densities of the PEG-rich phases of systems did not differ much with an increasing TLL. On the other hand, the densities of the citrate-rich phases showed a significant increase with the TLL. Refractive index of the PEG-rich phases increased linearly with TLL.The binodal curve generated was similar to previous work [38] and the tie lines determined were parallel, as expected, and are also shown in **Figure 1B**. The tie lines had an average slope of -1.6 ± 0.2. The PEG concentrations in the PEG-rich phase was measured by generating a standard curve (Table **S3**). The measured PEG concentrations showed a slight deviation from the previously determined tie lines using conductivity method. However, the standard curve was generated without adding citrate salt, which is present when two-phase systems are formed. Any system composition on a given tie line separates into the same respective PEG and salt compositions [57], only the volume ratio changes of each system. The TL ratios were indirectly proportional to the volume ratios (**Eq. 3**), as shown in **Table 3** thus suggesting an increase in the TL ratio will decrease the volume ratio.

3.3. Effect of tie lines & tie line length ratios

Three TLLs and at least three TL ratios were chosen to study the recovery of PPV and HRV with respect to phase composition and phase volume. The system matrix also explored the effect of phase composition changes on the partitioning behavior of contaminants, in particular host-cell proteins and DNA.

The shortest TLL studied was 15 w/w%. TLL 15 w/w% contained the lowest concentration of PEG and citrate of those tested. The lower compositions have relatively low hydrophobic interaction from the PEG-rich phase and low salting-out effect from the citrate-rich phase. It was observed that PPV highly partitioned to the citrate-rich phase and very little PPV was recovered in the PEG-rich phase, as shown in **Figure 2 A&B**. Recoveries in the citrate-rich

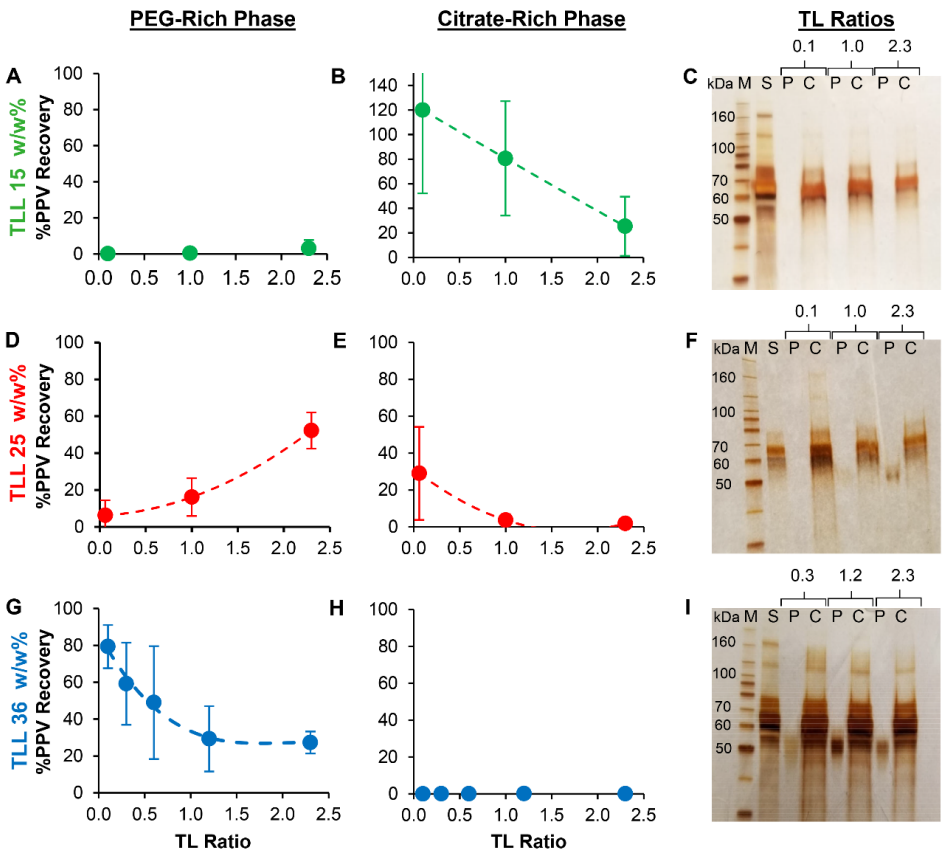

Figure 2. PPV recovery in the PEG-rich phase (left column) and the citrate-rich phase (middle column) at different TLL. SDS-PAGE (right column) of marker (M), starting PPV (S), the PEG-rich phase (P), and the citrate-rich phase (C) at different TLL and TL ratios. The starting titer was 6.5 MTT_{50}/ml. Experiments were done in triplicate and the error bars represent the standard deviation.

phase started at 100% at TL ratio 0.1 and decreased to 20% at TL ratio 2.3. Irrespective of the TL ratio, the contaminant proteins partitioned to the citrate-rich phase, as shown in **Figure 2C**. The PPV concentration is too low to be seen on an SDS-PAGE. Since there was not enough preferential partitioning of the PPV particles to the PEG-rich phase, the lower TLL is not suitable for the purification of PPV.

To increase the driving forces (i.e. salting-out of the citrate and hydrophobic interaction of the PEG) and obtain higher recovery of the viral particles in the PEG-rich phase, systems on TLL 25 w/w% were studied. As shown in **Figure 2D**, the PPV recovery in the PEG-rich phase increased almost linearly with the TL ratio. A maximum of 52% PPV was recovered in the PEG-rich phase at TL ratio 2.3. This corresponded to a decrease in recovery in the citrate-rich phase as the TL ratio increased (**Figure 2E**). However, the recoveries in the citrate-rich phase remained low at <30%. The remainder of the viral particles are likely aggregated at the interface or have been rendered noninfectious by the system and are not recoverable, as stated previously [38]. It is most likely that the virus has been trapped at the interface, since we do obtain high recoveries at TLLs with both increased and decreased concentrations of PEG and citrate.

Most of the contaminant proteins partitioned to the citrate-rich phase, as shown in **Figure 2F**. One contaminant protein partitioned along with PPV in the PEG-rich phase for TLL 25 w/w%, as seen by the band between 50 and 60 kDa. The decreasing band intensity with an increase in the TL ratio was observed in the citrate-rich phase, the cause of which might be the decreasing concentration of the proteins with an increasing volume of the citrate-rich phase, i.e. the citrate is diluting the protein. TLL 25 w/w% provided a better driving force for the preferential partitioning of PPV to the PEG-rich phase than TLL 15 w/w%.

The highest TLL studied was TLL 36 w/w%. It was hypothesized that higher recoveries in the PEG-rich phase depended on increasing the driving forces of salting-out from the citrate-

rich phase and the attractive interaction from the relatively hydrophobic PEG-rich phase. TLL 36 w/w% had the highest concentration of both PEG and citrate studied, and therefore, the highest driving force tested. It was observed that with an increasing TL ratio, the recoveries showed a declining trend in the PEG-rich phase for TLL 36 w/w% (**Figure 2G)**. On the contrary, the citrate-rich phase was almost void of PPV for all TL ratios studied for TLL 36 w/w% (**Figure 2H)**. A maximum of 79% PPV was recovered in the PEG-rich phase at TL ratio of 0.1. As demonstrated for the other tie lines, the contaminate proteins partitioned to the citrate-rich phase (**Figure 2I)**. One band between 50 & 60 kDa was observed in the PEG-rich phase similar to TL ratio 25 w/w%. Overall, higher recoveries were observed at TLL 36 w/w% than at TLL 25 w/w% for TL ratios <1. This is likely due to the high PEG concentration in the higher TLL, which provides a more suitable environment for PPV recovery. The DNA concentration was measured in the PEG-rich phase and citrate-rich phase to determine the partitioning of DNA at TLL 25 w/w% and 36 w/w%. At both the TLL studied, DNA was salted out of the citrate-rich phase (**Table 4**), demonstrated by recoveries less than 24% in the citrate-rich phase. On the other hand, the PEG-rich phase had an average of 24% of the initial stock host cell DNA at the lower TL ratio. The DNA recovery dropped for the higher TL ratio. Overall, the salted-out DNA appears to partition at the interface and is not recovered in the PEG-rich phase. This is similar

to what has been seen for partitioning of DNA in ATPS [81]. This demonstrates that ATPS has some DNA removal capability, but it is not a large DNA reducing step.

Similar studies were performed with HRV to determine the effect of viral surface charge on the partitioning and recovery of the virus. The recovery of HRV in the PEG-rich phase on TLL 15 w/w% remained low, almost 0% (**Figure 3A**). This low recovery was similar to PPV for TLL 15 w/w%. At the increased TLL of 25 w/w%, the HRV recovery increased to between 11 and 21%, depending on the TL ratio. Furthermore, TLL 36 w/w% provided an even stronger driving force where the recovery of HRV increased to 36% at TL ratio 0.3 (**Figure 3A**). The recovery of the HRV in the PEG-rich phase showed an opposite trend on TLL 25 w/w% and 36 w/w%. This trend was similar to the PPV behavior at the same TLLs, as shown in **Figure 2D&G**. Also, the HRV titers were almost identical to the PPV titers in the PEG-rich phase for all the systems studied (**Table S4**) suggesting that the highly hydrated citrate ions dehydrate the HRV surface which promotes the hydrophobic interaction of PEG-rich phase and dehydrated viral surface.

The citrate-rich phase titers were strongly affected by the presence of citrate in the samples. This is clearly seen in the citrate-rich phase recoveries, where the recoveries at TLL 15 w/w% and 25 w/w% were more than 150% at TL ratios >1. These high titers, which then resulted in high recoveries in the citrate-rich phase, were likely due to the interaction of the cells

Table 4. Host cell DNA recoveries in the PEG-rich phase and citrate-rich phase as a function of TLL and TL ratio

TLL (w/w%)	TL ratio	PEG-rich phase recovery (%)	Citrate-rich phase recovery (%)
25	0.1	25 ± 1	24 ± 0
	2.3	5 ± 3	21 ± 9
36	0.3	22 ± 22	22 ± 6
	2.3	18 ± 6	10 ± 2

Data is the average of experiments performed in triplicates and the error represents the standard deviation

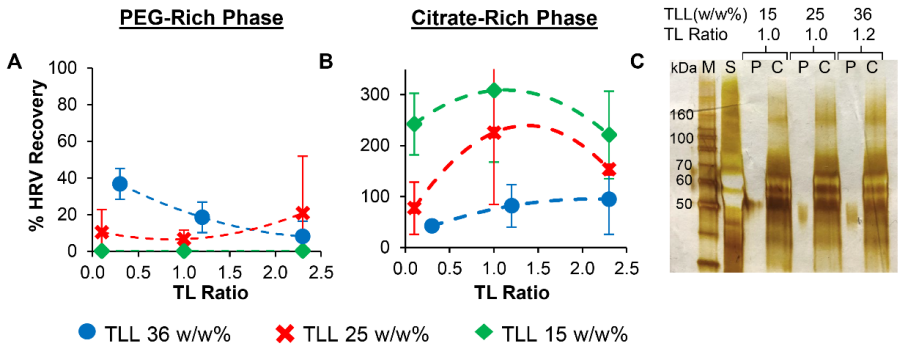

Figure 3. HRV recovery in the PEG-rich phase (A) and the citrate-rich phase (B) at different TLL. SDS-PAGE (C) of marker (M), starting HRV (S), PEG-rich phase (P) and the citrate-rich phase (C) at TLL 15, 25, and 36 w/w% with TL ratio 1.2. The starting titer was log 6.5 MTT_{50}/ml. Experiments were done in triplicate and the error bars represent the standard deviation.

with the citrate. Some groups have shown that citrate reduces cell viability [82] and is cytotoxic to cancer cells [83] at certain concentrations. Reduction of the cell viability increases the titer in the MTT assay as the virus quantification is based on the cell viability. An increase in the titer increases the recovery. The mass balance of viral particles held true only at TLL 36 w/w% with a total mass balance ranging between 77 and 102%. Overall, the HRV recovery followed the same trends as PPV. At low TLL, the virus remained in the citrate-rich phase and transitioned to the PEG-rich phase at the highest TLL studied.

Similar to PPV, the contaminant proteins present in the HRV solution were found mainly in the citrate rich phase (**Figure 3C**). The bands of the PEG-rich phase and citrate-rich phase corresponding to all the systems studied were identical. Hence, only one representative gel comprising of TLL 15, 25, and 36 w/w% at TL ratio 1.2 is shown (**Figure 3C**). The purity of the PEG-rich phase was similar to PPV. HRV partitioning demonstrated a high purity but low recovery as compared to the high purity and high recovery found with PPV.

3.4. Effect of increased PPV load

To understand the effect of loading, the initial PPV load was increased from 6.5 $\log_{10}$ MTT_{50}/ml, used in **Figure 2**, to 8 $\log_{10}$ MTT_{50}/ml. The loading effect was only performed with

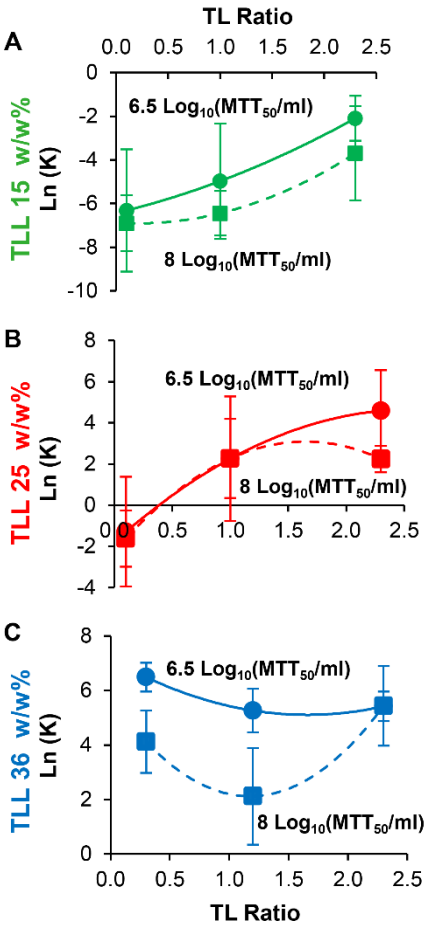

Figure 4. PPV partitioning at two different loading along TLL 15, 25, and 36 w/w%. Experiments were repeated in triplicates and error bars represent the standard deviation.

PPV as the highest titer of the HRV stock achieved was only 7 $\log_{10}$ MTT_{50}/ml. The PPV partitioning coefficient, *K* (**Eq. 5**), on all three TLLs showed similar trends for both loadings, as shown in **Figures 4 A**&**B**. TLL 15 and 25 w/w% showed increasing K values with respect to an increasing TL ratio and exhibited decreasing K values for TLL 36 w/w%. It was noted that the partitioning coefficient values are similar or lower for the higher load on all the TLLs. However, the virus titer increased in the PEG-rich phase by increasing the initial load for all the systems studied (**Table S5**). But a respective increase of virus titer in the citrate-rich phase suggested that a considerable number of viral particles still remained in the citrate-rich phase. This suggests that all the systems with an initial PPV load of 8 $\log_{10}$(MTT_{50}/ml) have higher ability

than systems with an initial PPV load of 6.5 $\log_{10}(MTT_{50}/ml)$ to drive viral particles in the PEG-rich phase, but the distribution of the viral particles is maintained to balance the free energy between the two-phases. In the previous studies, the free energy has been correlated to the partition coefficient suggesting that for a given system composition the partition coefficient should remain the same [31, 84].

4. Discussion

This study examined the partitioning of PPV and HRV in an ATPS of PEG 12kDa-citrate. The goal was to determine the influential driving forces in ATPS partitioning at pH 7. There are two main theories that explain the partitioning of biomolecules in ATPS, 1) the excluded volume effect [30, 42-44] and 2) hydrophobic and electrostatic interactions [45-47, 74]. A previous study conducted for PPV ATPS partitioning using various molecular weights of PEG, salt types and pHs supported the concept of viral surface and phase hydrophobicity as the main driving forces [38]. This work supports two main conclusions, 1) increasing the PEG and citrate concentration, and therefore increasing the phase hydrophobicity and salting-out effect, increases the PPV and HRV recovery in the PEG-rich phase at a constant pH and 2) the influence of the electrostatic interaction is vital in achieving the high recovery of viruses in the PEG-rich phase. Therefore, the data supports that in a PEG 12kDa-citrate system, electrostatics and hydrophobic interactions are the dominant forces.

The current theory for the partitioning of virus in ATPS involve the electrostatic interaction of the virus with the salt-rich phase and the hydrophobic interaction of the virus with the water-reduced, PEG-rich phase. The first interaction appears to be the salting-out of the virus from the citrate-rich phase. This is due to the charge repulsion of the citrate with the virus. PPV is negatively charged at pH 7, and when the salt concentration is raised from TLL 15 w/w% to TLL 25 w/w%, all of the PPV is salted-out of the salt-rich phase and is likely at the interface. When the PEG-rich phase concentration is increased to TLL 36 w/w%, there is enough

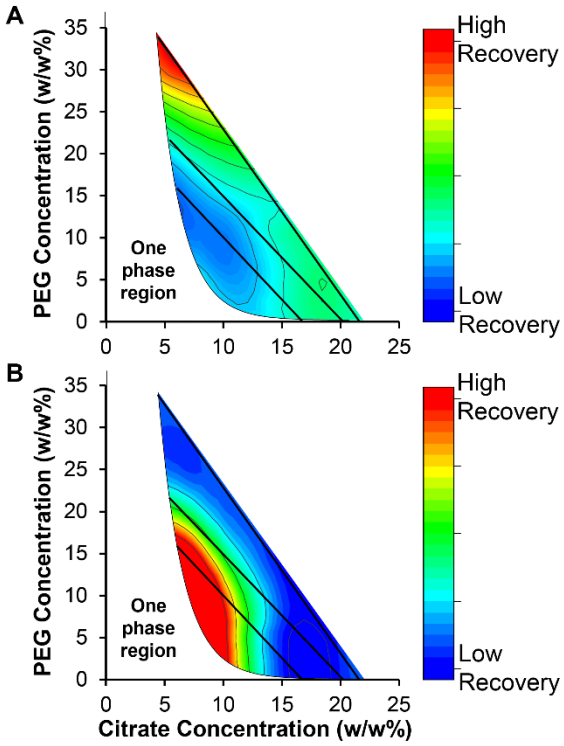

Figure 5. PPV recovery map in the two-phase region for (A) PEG-rich phase and (B) citrate-rich phase.

hydrophobic interaction driving force from the PEG-rich phase to extract the virus from the interface and have it recovered in the PEG-rich phase. This is illustrated by the recovery map shown in **Figure 5**. This theory is also supported by the data from HRV. HRV is neutrally charged at pH 7, and therefore does not experience the same amount of charge repulsion from the citrate-rich phase. Since the virus is not driven to the interface, it is not extracted from the interface by the PEG-rich phase. Therefore, our current hypothesis is that first the virus must be salted-out by charge repulsion from the salt-rich phase to the interface. Then the PEG-rich phase needs to be strong enough to extract the virus from the interface into the PEG-rich phase. The experiments described here never reached a citrate concentration that salted-out the contaminating proteins so that they could be extracted into the PEG-rich phase. This is preferred because it provides a difference in driving force needed to purify the viral particles.

The salting-out phenomena is the interaction of salt ions (electrolyte), biomolecules

(non-electrolyte) and solvent. At lower salt concentrations, the salt ions interact with the biomolecules by forming a layer of counter ions around the charged biomolecule. The counter ion layer increases the water structure stability and decreases the free energy, therefore promoting biomolecule solubility. An increase in the salt concentration, above a critical concentration, causes a high repulsion force to develop from the development of an electronic double layer and the close proximity of liked charged ions near the surface of the biomolecule [85]. This high repulsion force increases the free energy of the biomolecule surface, thereby making the surface thermodynamically unstable [86].

To test the effect of citrate concentration on the aggregation of PPV, DLS was measured for PPV in different citrate concentrations. Due to aggregates that were present in the starting material, an aggregation ratio was used to compare the intensity of the PPV peak and the aggregate peak. The full calculation is described in **Eq. 7**. PPV particles started to aggregate at 15 w/w% citrate, with extensive aggregation occurring at 20 w/w% and above (**Fig. S1**). 20 w/w% citrate and above are close to the citrate-rich phase compositions of the TLLs, 25 and 36 w/w%, studied (see **Fig. 1).** These results support the hypothesis that PPV is salted-out at high citrate concentration. Without the PEG-rich phase present (i.e. citrate only, as was conducted in the DLS experiments), PPV aggregated. In the presence of the PEG-rich phase, the PPV particles can reduce their free energy by migrating to the PEG-rich phase. Aggregation was not measured for HRV due to the low HRV titer available which was not detectable by DLS measurements.

The proposed theory of hydrophobicity as the main driving force in ATPS was based on recent studies that have shown viral particles to be relatively more hydrophobic than proteins [61, 87]. The PPV surface was shown to be more hydrophobic than the model proteins BSA, lysozyme, bovine fibrinogen, and human IgG, by studying reverse phase chromatography, ANS fluorescence, and the results were compared with computationally determined solvent exposed surface area [61]. Another team performed hydrophobic interaction chromatography (HIC)

studies on a variety of enveloped and non-enveloped mammalian viruses and protein models, where viruses eluted at lower citrate concentrations as compared to the model proteins, suggesting the relatively hydrophobic nature of the viruses studied [87]. One of the viruses studied was MVM. MVM and PPV are both parvoviruses, therefore complementing the idea that PPV is hydrophobic. Similarly, the ATPS described here was designed to utilize the hydrophobic property of PPV to induce preferential partitioning of the virions to the PEG-rich phase.

A few studies have been reported to measure the hydrophobicity or predict the partitioning behavior based on hydrophobicity of proteins [45], or peptides [47] in ATPS. The hydrophobic interaction in ATPS is driven by the PEG molecular weight and concentration. This growing evidence of the hydrophobic interaction as a vital driving force in ATPS could be reasoned by the molecular composition of PEG. The increase in the PEG molecular weight and/or concentration increases the number of ethyl groups in the polymer chain. Ethyl groups are hydrophobic and optimum number of monomers provide the necessary hydrophobic interaction binding sites to attract proteins or viruses [49]. The minimization of free energy increase of the biomolecules, from the salting-out effect, is compensated by the availablility of the free energy provided by the amount of $-CH_2-CH_2-$ groups in the PEG-rich phase. The high recoveries of virus in PEG-ctirate ATPS is possible by the right balance of salting-out and hydrophobic interaction.

5. Conclusions

This study reported the recoveries of PPV and HRV in a PEG 12kDa-citrate system at pH 7. The PPV and HRV titers in the PEG-rich phase increased with an increase in TLL. Most of the viral particles were recovered in the citrate-rich phase at TLL 15 w/w%, the lowest TLL studied. The PPV and HRV recovery in the PEG-rich phase increased at TLL 25 w/w%. Across this tie line, the PPV and HRV recovery increased in the PEG-rich phase as the TL ratio increased. TLL 36 w/w% showed the opposite trend; the recovery decreased as the TL ratio

increased. The highest PPV recovery of 74% and HRV recovery of 36% was found on TLL 36 w/w% and a TL ratio 0.1. An increase in the PPV titer yielded higher titers in the PEG-rich phase. Overall, this work supported the hypothesis that the main driving forces in viral particle ATPS are the salting-out from the citrate-rich phase followed by the hydrophobic interaction of the PEG-rich phase. Therefore, a higher TLL, leading to higher concentrations of salt and PEG, are needed for a high virus recovery in the PEG-rich phase.

The framework in this study achieves high virus recovery in a PEG-citrate system using known surface properties of the virus. The model viruses used demonstrated a need to understand the virus properties to improve virus recovery. By systematically studying the partitioning and recovery of negatively charged PPV and neutral HRV across tie lines, it was determined that the surface hydrophobicity and the charge at a given pH of the virus were key in the selective partitioning of the virus to the more hydrophobic PEG-rich phase. By combining the study of virus particle surfaces and the experimental ATPS design space, future correlations can be determined that will reduce the number of ATPS experiments needed to find an optimal system.

Acknowledgements

The authors thank NSF (CBET 1451959, 1510006, and 1818906), the James Lorna Mack Chair in Bioengineering, and Michigan Technological University for funding of this work. We acknowledge Henrietta Lacks and her surviving family members for the significant contributions that she and the HeLa cell line have made to scientific research and advances in human health.

Conflict of interest

The authors declare no conflict of interest.

References

1. WHO, *Global Vaccine Action Plan 2011-2020.* Global Vaccine Action Plan 2011-2020., 2013.
2. Shukla, A.A. and J. Thommes, *Recent advances in large-scale producaiton of monoclonal antibodies and related proteins.* Trends Biotechnol, 2010. **28**(5): p. 253-261.
3. Crosson, S.M., P. Dib, J.K. Smith, and S. Zolotukhin, *Helper-free Production of Laboratory Grade AAV and Purification by Iodixanol Density Gradient Centrifugation.* Mol Ther, 2018. **10**: p. 1-7.
4. Araldi, R.P., D.N. Giovanni, T.C. Melo, N. Diniz, J. Mazzuchelli-de-Souza, T.A. Sant'Ana, R.F. Carvalho, W. Becak, and R.C. Stocco, *Bovine papillomavirus isolation by ultracentrifugation.* J Virol Methods, 2014. **208**: p. 119-24.
5. Besnard, L., V. Fabre, M. Fettig, E. Gousseinov, Y. Kawakami, N. Laroudie, C. Scanlan, and P. Pattnaik, *Clarification of vaccines: An overview of filter based technology trends and best practices.* Biotechnol Adv, 2016. **34**(1): p. 1-13.
6. Robert, M.A., P.S. Chahal, A. Audy, A. Kamen, R. Gilbert, and B. Gaillet, *Manufacturing of recombinant adeno-associated viruses using mammalian expression platforms.* Biotechnol J, 2017. **12**(3).
7. Zhang, G., R. Deng, M. Zhao, S. Qiao, G. Xing, Y. Yang, Y. Wang, Q. Jin, J. Yang, L. Wang, Q. Li, J. Guo, Y. Zhi, and R. Wang, *Efficient purification of cell culture-derived classical swine fever virus by ultrafiltration and size-exclusion chromatography.* front agr sci eng, 2015. **2**(3).
8. Transfiguracion, J., H. Jorio, J. Meghrous, D. Jacob, and A. Kamen, *High yield purification of functional baculovirus vectors by size exclusion chromatography.* J Virol Methods, 2007. **142**(1-2): p. 21-8.
9. Bohua, L., S. Ming, Y. Lu, D. Xiaoyu, L. Baochun, S. Fenqin, Z. Li, and C. Xizhao, *Purification of porcine reproductive and respiratory syndrome virus using ultrafiltration and liquid chromatography.* J Chromatogr B Analyt Technol Biomed Life Sci, 2016. **1017-1018**: p. 182-186.
10. Auricchio, A., E. O'Connor, M. Hildinger, and J.M. Wilson, *A single-step affinity column for purification of serotype-5 based adeno-associated viral vectors.* Mol Ther, 2001. **4**(4): p. 372-4.
11. Du, P., S. Sun, J. Dong, X. Zhi, Y. Chang, Z. Teng, H. Guo, and Z. Liu, *Purification of foot-and-mouth disease virus by heparin as ligand for certain strains.* J Chromatogr B Analyt Technol Biomed Life Sci, 2017. **1049-1050**: p. 16-23.
12. Trilisky, E.I. and A.M. Lenhoff, *Sorption processes in ion-exchange chromatography of viruses.* J Chromatogr A, 2007. **1142**(1): p. 2-12.
13. Kalbfuss, B., M. Wolff, R. Morenweiser, and U. Reichl, *Purification of cell culture-derived human influenza A virus by size-exclusion and anion-exchange chromatography.* Biotechnol Bioeng, 2007. **96**(5): p. 932-44.
14. Nestola, P., C. Peixoto, R.R. Silva, P.M. Alves, J.P. Mota, and M.J. Carrondo, *Improved virus purification processes for vaccines and gene therapy.* Biotechnol Bioeng, 2015. **112**(5): p. 843-57.
15. Kramberger, P., L. Urbas, and A. Strancar, *Downstream processing and chromatography based analytical methods for production of vaccines, gene therapy vectors, and bacteriophages.* Hum Vaccin Immunother, 2015. **11**(4): p. 1010-21.
16. Allmaier, G., D. Blaas, C. Bliem, T. Dechat, S. Fedosyuk, I. Gosler, H. Kowalski, and V.U. Weiss, *Monolithic anion-exchange chromatography yields rhinovirus of high purity.* J Virol Methods, 2018. **251**: p. 15-21.
17. Krober, T., M.W. Wolff, B. Hundt, A. Seidel-Morgenstern, and U. Reichl, *Continuous purification of influenza virus using simulated moving bed chromatography.* J Chromatogr A, 2013. **1307**: p. 99-110.

18. Nestola, P., R.J. Silva, C. Peixoto, P.M. Alves, M.J. Carrondo, and J.P. Mota, *Adenovirus purification by two-column, size-exclusion, simulated countercurrent chromatography.* J Chromatogr A, 2014. **1347**: p. 111-21.
19. Zydney, A.L., *Perspectives on integrated continuous bioprocessing - opportunities and challenges.* Curr Opin Chem Eng, 2015. **10**: p. 8-13.
20. Zydney, A.L., *Continuous downstream processing for high value biological products: A Review.* Biotechnol Bioeng, 2016. **113**(3): p. 465-75.
21. Rito-Palomares, M., *Practical application of aqueous two-phase partition to process development for the recovery of biological products.* J Chromatogr B Analyt Technol Biomed Life Sci, 2004. **807**(1): p. 3-11.
22. Chethana, S., C.A. Nayak, M.C. Madhusudhan, and K.S. Raghavarao, *Single step aqueous two-phase extraction for downstream processing of C-phycocyanin from Spirulina platensis.* J Food Sci Technol, 2015. **52**(4): p. 2415-21.
23. Aguilar, O., V. Albiter, L. Serrano-Carreon, and M. Rito-Palomares, *Direct comparison between ion-exchange chromatography and aqueous two-phase processes for the partial purification of penicillin acylase produced by E. coli.* J Chromatogr B Analyt Technol Biomed Life Sci, 2006. **835**(1-2): p. 77-83.
24. Philipson, L., P.Å. Albertsson, and G. Frick, *The purification and concentration of viruses by aqueous polymer phase systems.* Virology, 1960. **11**(3): p. 553-571.
25. Luechau, F., T.C. Ling, and A. Lyddiatt, *Recovery of B19 virus-like particles by aqueous two-phase systems.* Food Bioprod Process, 2011. **89**(4): p. 322-327.
26. Benavides, J., J.A. Mena, M. Cisneros-Ruiz, O.T. Ramirez, L.A. Palomares, and M. Rito-Palomares, *Rotavirus-like particles primary recovery from insect cells in aqueous two-phase systems.* J Chromatogr B Analyt Technol Biomed Life Sci, 2006. **842**(1): p. 48-57.
27. Desai, R.K., M. Streefland, R.H. Wijffels, and M. H. M. Eppink, *Extraction and stability of selected proteins in ionic liquid based aqueous two phase systems.* Green Chem., 2014. **16**(5): p. 2670-2679.
28. Du, Z., Y.L. Yu, and J.H. Wang, *Extraction of proteins from biological fluids by use of an ionic liquid/aqueous two-phase system.* Chemistry, 2007. **13**(7): p. 2130-7.
29. Zeng, C.X., R.P. Xin, S.J. Qi, B. Yang, and Y.H. Wang, *Aqueous two-phase system based on natural quaternary ammonium compounds for the extraction of proteins.* J Sep Sci, 2016. **39**(4): p. 648-54.
30. Ho, S.L., J.C.-W. Lan, J.S. Tan, H.S. Yim, and H.S. Ng, *Aqueous biphasic system for the partial purification of Bacillus subtilis carboxymethyl cellulase.* Process Biochem, 2017. **58**: p. 276-281.
31. da Silva, N.R., L.A. Ferreira, P.P. Madeira, J.A. Teixeira, V.N. Uversky, and B.Y. Zaslavsky, *Analysis of partitioning of organic compounds and proteins in aqueous polyethylene glycol-sodium sulfate aqueous two-phase systems in terms of solute-solvent interactions.* J Chromatogr A, 2015. **1415**: p. 1-10.
32. Glyk, A., T. Scheper, and S. Beutel, *PEG–salt aqueous two-phase systems: an attractive and versatile liquid–liquid extraction technology for the downstream processing of proteins and enzymes.* Appl Microbiol Biotechnol, 2015. **99**(16): p. 6599-6616.
33. Asenjo, J.A. and B.A. Andrews, *Aqueous two-phase systems for protein separation: a perspective.* J Chromatogr A, 2011. **1218**(49): p. 8826-8835.
34. Jacinto, M.J., R.R.G. Soares, A.M. Azevedo, V. Chu, A. Tover, J.P. Conde, and M.R. Aires-Barros, *Optimization and miniaturization of aqueous two phase systems for the purification of recombinant human immunodeficiency virus-like particles from a CHO cell supernatant.* Sep Purif Technol, 2015. **154**: p. 27-35.
35. Noad, R. and P. Roy, *Virus-like particles as immunogens.* Trends Microbiol, 2003. **11**(9): p. 438-444.

36. González-Mora, A., F. Ruiz-Ruiz, J. Benavides, R.C. Willson, and M. Rito-Palomares, *Recovery and primary purification of bacteriophage M13 using aqueous two-phase systems.* J Chem Technol Biotechnol, 2017. **92**(11): p. 2808-2816.
37. Negrete, A., T.C. Ling, and A. Lyddiatt, *Aqueous two-phase recovery of bio-nanoparticles: a miniaturization study for the recovery of bacteriophage T4.* J Chromatogr B Analyt Technol Biomed Life Sci, 2007. **854**(1-2): p. 13-9.
38. Vijayaragavan, K.S., A. Zahid, J.W. Young, and C.L. Heldt, *Separation of porcine parvovirus from bovine serum albumin using PEG-salt aqueous two-phase system.* J Chromatogr B Analyt Technol Biomed Life Sci, 2014. **967**: p. 118-26.
39. Espitia-Saloma, E., P. Vázquez-Villegas, O. Aguilar, and M. Rito-Palomares, *Continuous aqueous two-phase systems devices for the recovery of biological products.* Food Bioprod Process, 2014. **92**(2): p. 101-112.
40. Vázquez-Villegas, P., O. Aguilar, and M. Rito-Palomares, *Continuous enzyme aqueous two-phase extraction using a novel tubular mixer-settler in multi-step counter-current arrangement.* Sep Purif Technol, 2015. **141**: p. 263-268.
41. Muendges, J., A. Zalesko, A. Gorak, and T. Zeiner, *Multistage aqueous two-phase extraction of a monoclonal antibody from cell supernatant.* Biotechnol Prog, 2015. **31**(4): p. 925-36.
42. Luechau, F., T.C. Ling, and A. Lyddiatt, *Selective partition of plasmid DNA and RNA in aqueous two-phase systems by the addition of neutral salt.* Sep Purif Technol, 2009. **68**(1): p. 114-118.
43. Gomes, G.A., A.M. Azevedo, M.R. Aires-Barros, and D.M.F. Prazeres, *Purification of plasmid DNA with aqueous two phase systems of PEG 600 and sodium citrate/ammonium sulfate.* Sep Purif Technol, 2009. **65**(1): p. 22-30.
44. Annunziata, O., N. Asherie, A. Lomakin, J. Pande, O. Ogun, and G.B. Benedek, *Effect of polyethylene glycol on the liquid-liquid phase transition in aqueous protein solutions.* Proc Natl Acad Sci U S A, 2002. **99**(22): p. 14165-70.
45. Andrews, B.A. and J.A. Asenjo, *Theoretical and Experimental Evaluation of Hydrophobicity of Proteins to Predict their Partitioning Behavior in Aqueous Two Phase Systems: A Review.* Sep Sci Technol, 2010. **45**(15): p. 2165-2170.
46. Grilo, A.L., M. Raquel Aires-Barros, and A.M. Azevedo, *Partitioning in Aqueous Two-Phase Systems: Fundamentals, Applications and Trends.* Sep Purif Rev, 2014. **45**(1): p. 68-80.
47. Eiteman, M.A. and J.L. Gainer, *Peptide hydrophobicity and partitioning in poly (ethylene glycol)/magnesium sulfate aqueous two-phase systems.* Biotechnol Prog, 1990. **6**(6): p. 479-484.
48. Guan, Y., T.H. Lilley, and T.E. Treffry, *A new excluded volume theory and its application to the coexistence curves of aqueous polymer two-phase systems.* Macromolecules, 1993. **26**(15): p. 3971-3979.
49. Wu, J., C. Zhao, W. Lin, R. Hu, Q. Wang, H. Chen, L. Li, S. Chen, and J. Zheng, *Binding characteristics between polyethylene glycol (PEG) and proteins in aqueous solution.* J Mater Chem B, 2014. **2**(20).
50. Silvério, S.C., A. Wegrzyn, E. Lladosa, O. Rodríguez, and E.A. Macedo, *Effect of Aqueous Two-Phase System Constituents in Different Poly(ethylene glycol)–Salt Phase Diagrams.* J Chem Eng Data, 2012. **57**(4): p. 1203-1208.
51. Mohamadi, H.S., E. Omidinia, and R. Dinarvand, *Evaluation of recombinant phenylalanine dehydrogenase behavior in aqueous two-phase partitioning.* Process Biochem, 2007. **42**(9): p. 1296-1301.
52. Hey, M.J., D.P. Jackson, and H. Yan, *The salting-out effect and phase separation in aqueous solutions of electrolytes and poly(ethylene glycol).* Polymer, 2005. **46**(8): p. 2567-2572.

53. Molitor, T.W., H.S. Joo, and M.S. Collett, *Porcine parvovirus: virus purification and structural and antigenic properties of virion polypeptides.* J Virol, 1983. **45**(2): p. 842-854.
54. Arnold, E., G. Vriend, M. Luo, J.P. Griffith, G. Kamer, J.W. Erickson, J.E. Johnson, and M.G. Rossmann, *The structure determination of a common cold virus, human rhinovirus 14.* Acta Crystallogr., Sect. A: Found. Crystallogr., 1987. **43**(3): p. 346-361.
55. Heldt, C.L., R. Hernandez, U. Mudiganti, P.V. Gurgel, D.T. Brown, and R.G. Carbonell, *A colorimetric assay for viral agents that produce cytopathic effects.* J Virol Methods, 2006. **135**(1): p. 56-65.
56. Tafur, M.F., K.S. Vijayaragavan, and C.L. Heldt, *Reduction of porcine parvovirus infectivity in the presence of protecting osmolytes.* Antiviral Res, 2013. **99**(1): p. 27-33.
57. Hatti-Kaul, R., *Aqueous Two-Phase Systems_ Methods and Protocols*. Methods in Biotechnology, ed. J.M. Walker. Vol. 11. 2000: Springer Science & Business Media.
58. Nielsen, J., L. Rønsholt, and K.J. Sørensen, *Experimental in utero infection of pig foetuses with porcine parvovirus (PPV).* Vet Microbiol, 1991. **28**(1): p. 1-11.
59. Joo, H.S., C.R. Donaldson-Wood, and R.H. Johnson, *Observations on the pathogenesis of porcine parvovirus infection.* Arch Virol, 1976. **51**(1): p. 123-129.
60. Simpson, A.A., B. Hebert, G.M. Sullivan, C.R. Parrish, Z. Zadori, P. Tijssen, and M.G. Rossmann, *The structure of porcine parvovirus: comparison with related viruses.* J Mol Biol, 2002. **315**(5): p. 1189-98.
61. Heldt, C.L., A. Zahid, K.S. Vijayaragavan, and X. Mi, *Experimental and computational surface hydrophobicity analysis of a non-enveloped virus and proteins.* Colloids Surf B, 2017. **153**: p. 77-84.
62. Johnson, S., K.A. Brorson, D.D. Frey, A.K. Dhar, and D.A. Cetlin, *Characterization of Non-Infectious Virus-Like Particle Surrogates for Viral Clearance Applications.* Appl Biochem Biotechnol, 2017. **183**(1): p. 318-331.
63. Weichert, W.S., J.S. Parker, A. Wahid, S.-F. Chang, E. Meier, and C.R.J.V. Parrish, *Assaying for structural variation in the parvovirus capsid and its role in infection.* Virology, 1998. **250**(1): p. 106-117.
64. Jacobs, S.E., D.M. Lamson, K. St George, and T.J. Walsh, *Human rhinoviruses.* Clin Microbiol Rev, 2013. **26**(1): p. 135-62.
65. Smith, T.J., M.J. Kremer, M. Luo, G. Vriend, E. Arnold, G. Kamer, M.G. Rossmann, M.A. McKinlay, G.D. Diana, and M.J. Otto, *The site of attachment in human rhinovirus 14 for antiviral agents that inhibit uncoating.* Science, 1986. **233**(4770): p. 1286-1293.
66. Rossmann, M.G., E. Arnold, J.W. Erickson, E.A. Frankenberger, J.P. Griffith, H.-J. Hecht, J.E. Johnson, G. Kamer, M. Luo, and A.G.J.N. Mosser, *Structure of a human common cold virus and functional relationship to other picornaviruses.* Nature, 1985. **317**(6033): p. 145.
67. Johnston, S.L., P.K. Pattemore, G. Sanderson, S. Smith, F. Lampe, L. Josephs, P. Symington, S.O. Toole, S.H. Myint, D.A.J. Tyrrell, and S.T. Holgate, *Community study of role of viral infections in exacerbations of asthma in 9-11 year old children.* BMJ, 1995. **310**: p. 1225-1229.
68. Yamaya, M. and H. Sasaki, *Rhinovirus and asthma.* Viral Immunol, 2003. **16**(2): p. 99-109.
69. Friedlander, S.L. and W.W. Busse, *The role of rhinovirus in asthma exacerbations.* J Allergy Clin Immunol, 2005. **116**(2): p. 267-273.
70. Palmenberg, A.C. and J.E. Gern, *Classification and evolution of human rhinoviruses.* Methods Mol Biol, 2015. **1221**: p. 1-10.
71. Heikkinen, T. and A. Järvinen, *The common cold.* the Lancet, 2003. **361**(9351): p. 51-59.
72. Kim, S.R., J.H. Song, J.H. Ahn, G.S. Lee, H. Ahn, S.I. Yoon, S.G. Kang, P.H. Kim, S.M. Jeon, E.J. Choi, S. Shin, Y. Cha, S. Cho, D.E. Kim, S.Y. Chang, and H.J. Ko, *Antiviral*

and anti-inflammatory activity of budesonide against human rhinovirus infection mediated via autophagy activation. Antiviral Res, 2018. **151**: p. 87-96.
73. Wysoczanska, K., H.T. Do, C. Held, G. Sadowski, and E.A. Macedo, *Effect of different organic salts on amino acids partition behaviour in PEG-salt ATPS.* Fluid Phase Equilib, 2018. **456**: p. 84-91.
74. Goja, A., H. Yang, M. Cui, and C. Li, *Aqueous Two-Phase Extraction Advances for Bioseparation.* J Bioprocess Biotech, 2013. **04**(01).
75. de Oliveira, C.C., J.S.d.R. Coimbra, A.D.G. Zuniga, J.P. Martins, and A.M.d.O. Siqueira, *Interfacial Tension of Aqueous Two-Phase Systems Containing Poly(ethylene glycol) and Potassium Phosphate.* J Chem Eng Data, 2012. **57**(6): p. 1648-1652.
76. Perumalsamy, M. and T. Murugesan, *Phase Compositions, Molar Mass, and Temperature Effect on Densities, Viscosities, and Liquid−Liquid Equilibrium of Polyethylene Glycol and Salt-Based Aqueous Two-Phase Systems.* J Chem Eng Data, 2009. **54**(4): p. 1359-1366.
77. Chakraborty, A. and K. Sen, *Impact of pH and temperature on phase diagrams of different aqueous biphasic systems.* J Chromatogr A, 2016. **1433**: p. 41-55.
78. Wysoczanska, K. and E.A. Macedo, *Influence of the Molecular Weight of PEG on the Polymer/Salt Phase Diagrams of Aqueous Two-Phase Systems.* J Chem Eng Data, 2016. **61**(12): p. 4229-4235.
79. Huddleston, J.G., H.D. Eillauer, and R.D. Rogers, *Phase Diagram Data for Several PEG + Salt Aqueous Biphasic systems.* J Chem Eng Data, 2003. **48**(5): p. 1230-1236.
80. Tubío, G., L. Pellegrini, B.B. Nerli, and G.A. Picó, *Liquid−Liquid Equilibria of Aqueous Two-Phase Systems Containing Poly(ethylene glycols) of Different Molecular Weight and Sodium Citrate.* J Chem Eng Data, 2006. **51**(1): p. 209-212.
81. Nazer, B., M.R. Dehghani, and B. Goliaei, *Plasmid DNA affinity partitioning using polyethylene glycol - sodium sulfate aqueous two-phase systems.* J Chromatogr B Analyt Technol Biomed Life Sci, 2017. **1044-1045**: p. 112-119.
82. Garland, E.M., J.M. Parr, D.S. Williamson, and S.M. Cohen, *In vitro cytotoxicity of the sodium, potassium and calcium salts of saccharin, sodium ascorbate, sodium citrate and sodium chloride.* Toxicol in Vitro, 1989. **3**(3): p. 201-205.
83. Lu, Y., X. Zhang, H. Zhang, J. Lan, G. Huang, E. Varin, H. Lincet, L. Poulain, and P. Icard, *Citrate induces apoptotic cell death: a promising way to treat gastric carcinoma?* Anticancer Research, 2011. **31**(3): p. 797-805.
84. de Barros, D.P., S.R. Campos, A.M. Azevedo, A.M. Baptista, and M.R. Aires-Barros, *Predicting protein partition coefficients in aqueous two phase system.* J Chromatogr A, 2016. **1470**: p. 50-58.
85. Bostrom, M., F.W. Tavares, S. Finet, F. Skouri-Panet, A. Tardieu, and B.W. Ninham, *Why forces between proteins follow different Hofmeister series for pH above and below pI.* Biophys Chem, 2005. **117**(3): p. 217-24.
86. Queiroz, J.A., C.T. Tomaz, and J.M.S. Cabral, *Hydrophobic interaction chromatography of proteins.* J Biotechnol, 2001. **87**(2): p. 143-159.
87. Johnson, S.A., A. Walsh, M.R. Brown, S.C. Lute, D.J. Roush, M.S. Burnham, and K.A. Brorson, *The step-wise framework to design a chromatography-based hydrophobicity assay for viral particles.* J Chromatogr B Analyt Technol Biomed Life Sci, 2017. **1061-1062**: p. 430-437.